Resonant-photoemission study of SnO_2: Cationic origin of the defect band-gap states

J. M. Themlin, R. Sporken,* J. Darville, R. Caudano,* and J. M. Gilles
Laboratoire de Spectroscopie Moléculaire de Surface (LASMOS), Institute for Studies in Interface Sciences (ISIS), Facultés Universitaires Notre Dame de la Paix, 61 rue de Bruxelles, B-5000 Namur, Belgium

R. L. Johnson
II. Institut für Experimentalphysik, Universität Hamburg, Luruper Chaussee 149, D-2000 Hamburg 50, West Germany

(Received 14 May 1990)

The electronic properties of tin dioxide single-crystalline (110) surfaces have been studied in correlation with their structure by low-energy electron diffraction, angle-integrated and resonant photoemission using synchrotron radiation [ultraviolet photoemission spectroscopy (UPS)]. Energy distribution curves were measured from the Sn 4*d* core levels and from the valence band. The experimental valence band is compared with the theoretical density of states (DOS) from perfect and defective surfaces. UPS difference curves, normalized to the Sn 4*d* intensity, reflect mainly the increase in the oxygen partial DOS when the sample is annealed at increasing temperatures up to 1000 K after sputtering. Their comparison with simulated theoretical difference curves favors a bridging oxygen termination for annealing temperatures above 900 K. After argon-ion bombardment, band-gap defect states that are not predicted by the calculations are found at a maximum density 1.4 eV above the valence-band maximum (VBM). Various degrees of resonant enhancement occur throughout the valence band when the photon energy crosses the Sn $4d \rightarrow 5p$ photoabsorption threshold, and these are used to establish the tin-derived character of the gap states, for which a tin 5*s* origin is proposed. Partial-yield spectra allow the localization of unoccupied Sn 5*p* states in the conduction band starting from 8 eV above the VBM with a maximum at 10 eV. The Sn $4d \rightarrow 5p$ absorption threshold also shows possible core exciton formation for sputtered surfaces only.

I. INTRODUCTION

The knowledge of the electronic band structure of a compound is a basic requirement for a thorough understanding of its electro-optical properties. In particular, the electronic structure of semiconducting oxide surfaces is at present a subject of intense experimental and theoretical activity,[1,2] because the electronic properties of the surface can significantly differ from the bulk. In the case of tin dioxide (SnO_2), these surface properties have a crucial influence in technological applications, such as gas-sensing devices,[3] high-efficiency solar cells,[4] and catalysts.[5] The study of the nature and origin of resonances and surface states at SnO_2 surfaces is, therefore, of both fundamental and practical interest.

In this paper we report the results of angle-integrated and resonant photoemission using synchrotron radiation on SnO_2(110) surfaces. We present a résumé on the present state of knowledge about the electronic structure of these surfaces in Sec. II. Currently, the valence-band width and the atomic origin of the band-gap states for reduced surfaces are pressing questions to be answered. We describe our experimental procedure in Sec. III. We present in Sec. IV the results concerning the valence band (VB) and shallow core levels and discuss them in terms of bulk density of states (DOS) and surface electronic structure theory. Section V analyzes the changes induced by the surface treatment. Partial-yield spectra, which allow the study of the optical absorption and, therefore, the investigation of the unoccupied electronic states in the conduction band, are reported in Sec. VI. Resonant photoemission provides clear indications on the origin of the defect-related surface states that appear in the band gap after ion bombardment. These results are discussed in Sec. VII, while Sec. VIII gives the conclusions.

II. ELECTRONIC STRUCTURE OF SnO_2(110) SURFACES

SnO_2 is an *n*-type, wide-band-gap semiconductor ($E_g = 3.6$ eV) which crystallizes in the rutile structure, with six atoms per tetragonal unit cell. The electro-optical properties and growth modes have been reviewed some time ago,[6] and the bulk electronic structure of SnO_2 has been calculated by Robertson[7] and by Munnix and Schmeits.[8] Both exploit the tight-binding (TB) method based on O 2*s* and 2*p* orbitals and Sn 5*s* and 5*p* orbitals.

The scattering theoretical method has been used by Munnix and Schmeits to describe changes in the DOS arising from the presence of a surface, in particular, for the (110) orientation.[8] At least two different planes could terminate the crystal. The one most densely packed contains two Sn atoms with inequivalent coordination (4 and 5) and two oxygen anions per surface unit cell. In order to break the smallest number of cation-anion bonds,[1] it is necessary to add an atomic plane containing one oxygen atom per unit cell above the most compact plane. In this way the crystal is terminated by a nonpolar surface, while in the first case the last plane carries two positive elementary charges per surface unit cell. Due to the creation of

 ©1990 The American Physical Society

these two kinds of surfaces, the surface DOS changes as follows:[8] (a) "Backbond states" of dominant Sn character modify the DOS in a region between -7.5 and -5 eV below the valence-band maximum (VBM); (b) oxygen-$2p$-derived resonances change the DOS mostly in the region between -4 and 0 eV. These resonances are smaller for the nonpolar termination than for the more compact one; (c) the band gap is free of surface states. This fact has been related to the relatively strong ionicity of SnO_2. The influence of various types of point defects on the same surface has also been studied by the same group.[8] They found that the backbond states and resonances characteristic of the perfect surface are enhanced, and that the configurations they considered do not induce any defect states in the optical gap.

The first extensive experimental study of SnO_2 surfaces was performed by de Frésart, Darville, and Gilles.[9] They examined ion-bombarded and annealed surfaces using Auger electron spectroscopy (AES), LEED, electron energy-loss spectroscopy (EELS) together with contact potential difference (CPD), and sheet conductance measurements. Their analysis favored the most compact plane as the actual termination, and a number of thermally driven reconstructions were reported, depending on the annealing temperature after sputtering, namely (4×1), $c(1\times1)$ [which is actually $c(2\times2)$], (1×1), and (1×2). Thereafter, Cox, Fryberger, and Semancik have shown[10] by a combined ion scattering spectroscopy (ISS) and UPS study that the nonpolar termination could only be obtained after thermal annealing at 700 K in an elevated oxygen partial pressure of 100 Pa. They also showed that heating this surface in vacuum at temperatures as low as 500 K led to the removal of oxygen atoms from the outermost plane (creation of "bridging" oxygen vacancies.) Cox and co-workers have correlated these vacancies with the appearance of defect states in the band gap near the VBM.[10] This is in agreement with earlier UPS studies by Egdell, Eriksen, and Flavell[11] and Cox *et al.*,[12] who suggested that these defect states near the VBM are due to a $5s$-$5p$ rehybridization at tin sites. Half the tin ions in the outermost compact plane would be doubly ionized (Sn^{2+} instead of Sn^{4+} in the bulk) and would leave the compact-plane termination uncharged, thus providing a local SnO-like configuration. We will use this purely ionic description of the formal oxidation state throughout this work. However, this is only a simplified picture, as the covalent interactions between oxygen and metal induce charge sharing in addition to ionic bonding.

The pioneering work on $SnO_2(001)$ using UPS by Gobby and Lapeyre[13(a)] should be mentioned in this context. They interpreted their photoemission spectra in terms of the bulk DOS, but the photon energy range was restricted to $h\nu < 30$ eV for the angle-integrated EDC's, so it was not possible to discriminate completely between the valence-band features and the secondary electron tail.

III. EXPERIMENTAL PROCEDURES

A. Apparatus

The photoemission experiments were performed on the FLIPPER-II monochromator at HASYLAB (DESY) in Hamburg, using ultraviolet and soft-x-ray light from the DORIS-II storage ring. The ultra-high-vacuum system consists of a small introduction chamber, a larger preparation chamber, and the analysis chamber, with base pressures ranging, respectively, from 10^{-8} to 10^{-9} Pa. In the analysis chamber, a cylindrical mirror analyzer (CMA), operated at 15-eV pass energy, was used to obtain angle-integrated photoemission spectra. The spectrometer work function was obtained by measuring the Fermi level of a metallic sample (freshly sputtered sample holder or Sn-rich SnO_2 surfaces) and yielded a value of 4.9 eV. The overall energy resolution (monochromator plus analyzer) ranged from about 0.3 eV, at $h\nu=25$ eV, to 0.5 eV, at $h\nu=90$ eV. At these energies, the escape depth of the photoelectrons is expected to be less than about 10 Å,[14] making our spectra highly sensitive to the surface DOS of the sample. The incoming light was incident at about 60° to the surface normal, giving mixed *s* and *p* polarization for the photon beam. The normal to the surface of the sample, its crystallographic *c* axis, the analyzer symmetry axis, and the incoming light beam direction were all in the horizontal plane. Further details of the experimental setup have been published elsewhere.[15] In addition to the usual energy distribution curves (EDC), spectra were also measured in the constant-final-state (CFS) mode. Resonance profiles were inferred from a series of EDC's at various photon energies. In both cases, each spectrum was normalized to the photon flux, the latter being independently determined using a calibrated photodiode.

B. Sample preparation

The tin dioxide single crystals used in this experiment were grown in our laboratory by the reactive vapor phase transport method used by Thiel and Helbig.[16] They consist of hollow needles oriented along the *c* axis, from which a single platelet was cut, using a diamond saw, to typical dimensions of $4\times12\times1$ mm^3. No additional treatments, other than degreasing in acetone, methanol, rinsing in deionized water, and drying under a nitrogen flux, were made on the (110) face, which was studied without additional polishing. The bulk resistivity of similar samples taken at room temperature was on the order of 10^6 Ω m. Four samples were used to check the reproducibility of the results. The sample was clamped with small stainless-steel springs to a sample holder equipped with a heating filament. The as-grown $SnO_2(110)$ surfaces were cleaned *in situ* by 500-eV argon-ion bombardment. The validity of the Ar^+ sputtering has been previously established. This sputtering yields no detectable impurities by AES.[9] Furthermore, no sign of contamination was found in our valence-band EDC's. To restore an ordered surface, the sample was heated under UHV for, typically, 30 min. at temperatures ranging from 400 up to 1000 K. The heating temperature was experimentally determined using an optical pyrometer pointing toward the stainless-steel plate through the transparent sample, assuming that the latter came to thermal equilibrium with the plate during heating.

All the photoelectron spectra were measured after

cooling the sample at room temperature, and after characterizing the surface crystallography using LEED. It is known that, depending on the annealing temperature, different surface reconstructions can be obtained and observed by LEED.[9] Our results apply to (110) surfaces prepared in the following ways: (a) just after sputtering, where only a diffuse background was detected by LEED; (b) sputtering followed by annealing around 800 K, which yielded good LEED patterns with a (4×1) reconstruction; (c) sputtering followed by heating at temperatures around 900 K, where sharp LEED spots with a (1×1) structure were observed; (d) sputtering followed by heating at higher temperatures around 1000 K, which also produced the (1×1) structure. The (1×1) LEED pattern is expected for a simple termination of the bulk lattice.

IV. VALENCE-BAND PHOTOEMISSION AND SHALLOW CORE LEVELS

A. Valence band

A typical valence-band EDC for $SnO_2(110)$, taken at 40-eV photon energy after annealing at 1000 K, is shown in Fig. 1. The overall shape of the curve is in good agreement with the theoretical bulk DOS derived by Robertson,[7] using the tight-binding method. Munnix and Schmeits[8] described the unperturbed bulk SnO_2 crystal by a slightly modified, more realistic parameter set for the empirical tight-binding Hamiltonian. The theoretical valence-band DOS,[17] which was adjusted to fit the width of the early UPS data of Gobby,[13(b)] is also displayed in Fig. 1. In order to compare with the experimental photoemission spectra, the calculated VB DOS must be convoluted with a Gaussian-Lorentzian function to account for the finite lifetime and instrumental resolution broadenings, but neglecting any photoionization cross-section effects. The broadened DOS is also given in Fig. 1. Three distinct features can be clearly identified in the valence-band EDC. The first part of the VB, at binding energies (E_b) between 0 and 2 eV, results from bands which have mainly oxygen $2p$ bonding or nonbonding character. Intermediate states between 2.0 and 5.5 eV originate mainly from $pp\sigma$ hybridization between Sn $5p$ and O $2p$ orbitals. The lower part of the VB results from strong interactions between Sn $5s$ and O $2p$ (bonding) orbitals. If the upper 0-$2p$-derived bands are more ionic in nature, the other ones are more covalent, showing considerable s-p or p-p mixture in the bulk wave functions. Figure 1 also shows the broadened local DOS integrated on a cluster of surface and subsurface atoms for the (110) compact termination. The overall agreement with the experimental EDC is improved, especially for binding energies (E_b) between 1.5 and 3 eV, where localized oxygen resonances strongly affect the DOS. Furthermore, the third part of the VB peaks at $E_b=6.9$ eV, both in the surface-DOS and in the EDC. The corresponding feature for the bulk VB DOS peaks at $E_b=7.7$ eV, and also ends at higher E_b. This difference results from the suppression of Sn $5s$–O $2p$ interactions when a surface is created.[8]

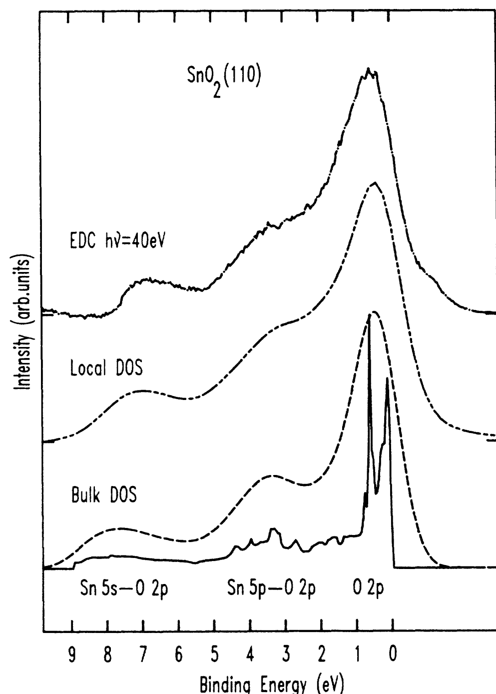

FIG. 1. Valence-band structure of SnO_2. Lower curves: calculated bulk DOS of SnO_2 (solid line); convoluted with a Gaussian of HWHM 0.53 eV (dashed line). Middle curve: local DOS's summed on a cluster of atoms (Ref. 8) for the (110) face with a bridging-oxygen termination (see text for definition). The calculations were performed with a Lorentzian broadening of 0.30 eV (Ref. 8), and the result has been further convoluted with a Gaussian (HWHM, 0.44 eV). Upper curve: a typical energy distribution curve measured at $h\nu=40$ eV after sputtering and annealing at 1000 K. The background due to inelastically scattered electrons has been subtracted. The binding energies are given relative to the valence-band maximum. All the curves are aligned to the VBM and normalized to the O $2p$ peak height.

The origin of our binding energies was set at the VBM at the surface, as usual for semiconductors.[18] The VBM was preferred to the Fermi level (E_F) as a reference energy, because the DOS inside the band gap is generally too low for an accurate determination of E_F at the photoemission threshold. Furthermore, for the kinetic energies used in this work, photoemission is highly surface sensitive, so that any band bending can change the value of E_F with respect to the band edges. It should be pointed out that a precise determination of the VBM is important in order to locate correctly the position of surface states and of other transitions, which we will discuss in detail. The location of the VBM in our UPS data was complicated by the presence of a slowly varying photoelectron signal, resulting from a surface-state band. One possibility is to extrapolate the tangent to the low-E_b side of the O $2p$ peak until it crosses the energy axis, and to define the intercept as the VBM. This procedure was employed for some semiconductors, and its validity is supported by the more elaborate approach of Kraut et al.[19] These authors modeled their x-ray photoemission spectroscopy (XPS) VB spectra in the vicinity of the VBM by an instrumentally broadened theoretical VB DOS adjusted to the experimental data using a least-squares method. For SnO_2, the rapid variation of the bulk or surface DOS at the VBM does not allow the extrapolation of the tangent line

to be a good approximation of the VBM. Unlike in elemental or III-V semiconductors,[20] the high DOS in the upper part of the VB seems to preclude such a simple approach. We, therefore, compare our experimental data in the vicinity of the VBM with theoretical simulations. The theoretical surface-VB DOS was convoluted with a Gaussian instrumental resolution function $g(E)$. The position of the VBM corresponds to the onset of the theoretical DOS, which have been obtained using a Lorentzian broadening of 0.30 eV. The energy difference between the VBM and the extrapolation of the tangent was determined, together with the half-width at half maximum (HWHM) of the O $2p$ peak. This procedure was repeated for several values of the $g(E)$ HWHM. It was found that the intercept was systematically displaced toward lower binding energies with respect to the true VBM, and that the difference is linear with respect to $g(E)$ HWHM. The simulated O $2p$ HWHM is quadratic with respect to $g(E)$ HWHM. The experimental O $2p$ HWHM was taken on the low-E_b side of the peak, in order to avoid the photon-energy-dependent changes in the intensity of the adjacent peak. In this way the actual $g(E)$ HWHM could be obtained as a function of photon energy. It ranges from 0.3 eV, at $h\nu=25$ eV, to 0.5 eV, at $h\nu=90$ eV. The energy difference between the VBM and the tangent increases linearly with respect to the $g(E)$ HWHM from 0.8 to 1.1 eV. Thus the practical procedure used was the following: For each experimental spectrum, we first perform the linear extrapolation of the tangent line to the low-E_b side of the O $2p$ peak. The intercept with the abscissa gives us a value from which we subtract the energy difference determined above, obtaining a more reliable estimate of VBM.

The high-E_b limit of the VB was taken at the inflection point of the EDC near $E_b=7.5$ eV, since the DOS in this region is small and varies smoothly. Using this procedure, the measured VB width is 7.5 eV, roughly 1 eV smaller than the results of Gobby and Lapeyre,[13] but 2 eV smaller than the calculated value of Robertson.[7] The valence-band (VB) widths and band-gap energies found by different theoretical methods are given in Table I. While the TB calculations involve moving the band extrema in order to fit photoemission or optical data, they are the only ones that predict the correct symmetry and type of band gap (direct at Γ, optically forbidden).[7] Svane and Antoncik[23] have recently applied the scalar-relativistic linear muffin-tin orbital (LMTO) method to obtain the band structure of some dioxides from first principle calculations. However, their results which take into account exchange and correlation yield a VB width of only 6.6 eV. These authors claimed that the experimental value of Gobby and Lapeyre for the VB width was not particularly firmly established. It is true that, in addition to the experimental difficulty of determining the VBM position, the photon energies used by Gobby in the angle-integrated EDC's only ranged from 11 to 30 eV. The last part of the VB was thus buried in the secondary electron tail. Our experimental data, however, provide clear evidence that the VB width is 7.5 eV. The methods based on the muffin-tin approximation seem to fail in obtaining a detailed positioning of the bands, although the overall shape qualitatively agree with the VB DOS determined using TB methods. It is interesting to note that the same trends were described for Cu_2O, where a self-consistent Gaussian orbital calculation underestimates the optical gap and the width of the O $2p$ bands.[24]

B. Tin 4*d* core level

Figure 2 shows the characteristic results of the spin-orbit split Sn $4d$ core levels, which appear as a poorly resolved doublet around 22-eV binding energy. In contrast to metallic tin, the two components of the $4d$ levels cannot be resolved. In the oxide, the inhomogeneous charging effects and the reduced core-hole lifetime, due to the larger density of valence electrons, increase the width of the two peaks. For the (1×1) surface annealed at 1000 K, the FWHM is 1.9 eV, and the $4d_{3/2}$ level is clearly visible as a shoulder on the high-E_b side. We find an E_b of 23.2 eV for Sn $4d_{3/2}$, and 22.2 eV for Sn $4d_{5/2}$. This gives a spin-orbit splitting of 1.0 eV, in agreement with the tabulated value of 1.0 eV,[18] and an intensity ratio between the two components of about 3/2, the statistically expected value. Following argon-ion bombardment, the FWHM increases slightly to 2.1 eV, and the $4d_{3/2}$ shoulder disappears. We found it impossible to fit the latter spectrum by increasing merely the width of each component of the doublet previously identified. Good

TABLE I. Valence-band widths and forbidden band-gap energies found by different theoretical methods.

Authors	Method	VB width (eV)	E gap (eV)
Arlinghaus[a]	Self-consistent, APW	5.3	2.62 (indirect)
Jacquemin, Bordure[b]	Korringa-Kohn-Rostoker (KKR)	10.0	3.6 (direct)
Svane, Antoncik[c]	LMTO	6.6	3.69 (indirect)
Robertson[d]	Tight binding	10.0	3.6 (direct)
Munnix, Schmeits[e]	Tight binding	9.0	3.6 (direct)

[a]Reference 21.
[b]Reference 22.
[c]Reference 23.
[d]Reference 7.
[e]Reference 8(b).

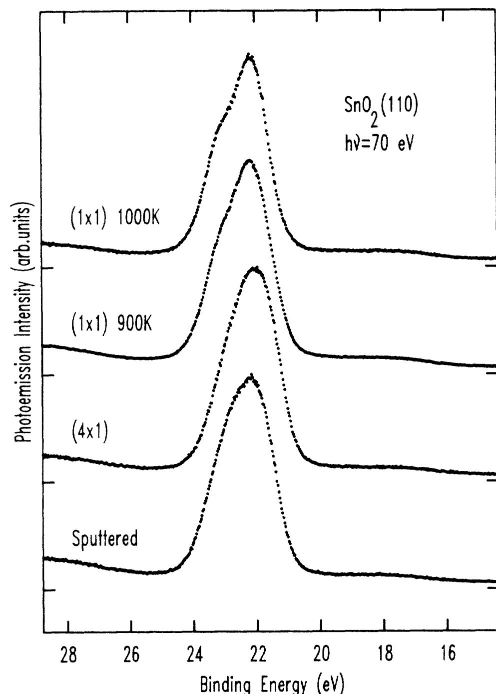

FIG. 2. Sn 4d core-level energy distribution curves from SnO_2(110) taken at a photon energy of 70 eV after sputtering and annealing at increasing temperatures (see text for details). The spectra have been normalized to equal height. The binding-energy scale refers to the valence-band maximum.

agreement was obtained by adding a second doublet with a higher ratio. This second doublet could possibly arise from the reduced Sn^{2+} species present at the sputtered surface, and would also contribute to a smaller extent to the 4d emission from the (4×1) and (1×1) 900 K surfaces. It must be stressed that, even after strong ion bombardment, we did not observe any structures characteristic of metallic tin homogeneously distributed on the whole surface. This is also true for a partly reconstructed surface (characterized by some LEED spots) and for the (4×1) reconstruction. This is different with the behavior of isostructural TiO_2 (Ref. 25) under ion bombardment, which shows not only significant nonstoichiometry but also excess metal as seen in the core-level spectra. However, we did observe in some marginal cases (on the edge of a sample or after strong heating of a freshly introduced sample) two additional peaks due to metallic tin, separated from their oxide counterparts by 2.5 eV toward lower binding energies. These observations seem to favor isolated surface oxygen vacancies (F_s centers) as the most probable defect created by low-energy ion bombardment, for in none of our standard surface preparations have we observed the clustering of Sn atoms. This is in agreement with the results found by other authors.[10] Clustering could, perhaps, happen at higher ion energies. Indeed, a recent study on cobalt oxide[26] showed that, in order to create more complicated defects than isolated oxygen vacancies at the surface, it was necessary to use higher energies (5000 eV) for ion bombardment.

V. EFFECT OF SURFACE TREATMENT

As shown in Fig. 3, the electronic structure of the SnO_2 surface is fairly sensitive to the surface treatment conditions. Indeed, AES measurements[9] have indicated that ion or electron bombardment induces a preferential sputtering of oxygen species at the surface. This reduction process introduces band-gap states. In our results, the photoemission intensity does not fall to zero in the band gap, even when a sharp (1×1) LEED pattern is observed. According to the findings of Cox and coworkers,[10] this is due to the fact that band-gap states occurring on the surface have not been removed by subsequent annealing in oxygen. The intensity of the band-gap states shoulder is maximum after extended ion bombardment. Subsequent UHV annealing at temperatures up to 1000 K reduces the density of these states. The latter can then be described as a single peak, situated 1.4 eV above VBM, appearing as a marked shoulder on the low-E_b side of the O 2p peak. Figure 3 shows the magnified contribution from the band-gap states, which

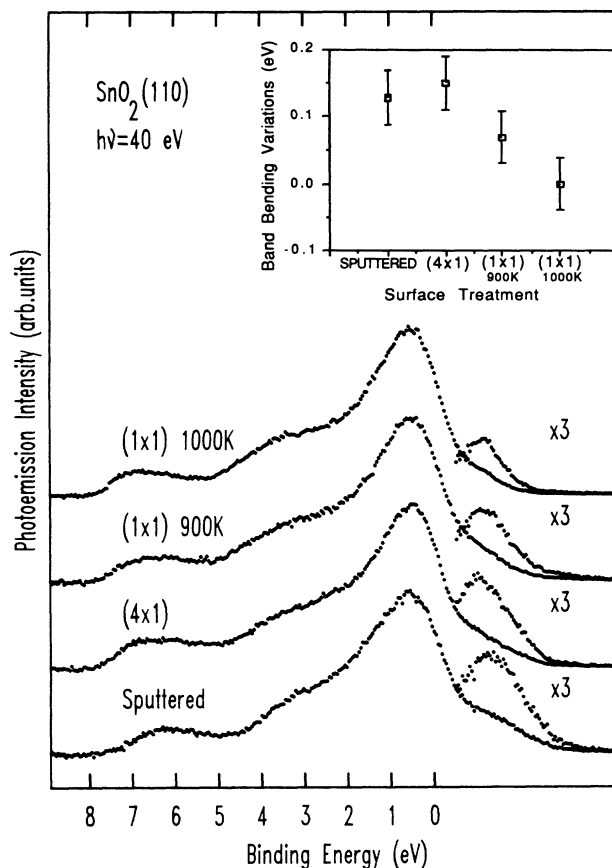

FIG. 3. Valence-band EDC's at $h\nu=40$ eV from SnO_2(110) after sputtering and annealing at increasing temperatures (see text for details). The spectra are normalized to an equal height of the 0 2p peak. The magnified contribution from the band-gap states has been extracted by subtracting half a Gaussian adjusted to the low-E_b side of the O 2p peak from the experimental data. The inset shows the relative variations of the band bending at the surface. The VBM location for the surface annealed at 1000 K has been chosen as the reference level.

has been extracted as follows. First, half a Gaussian of appropriate HWHM, corresponding to the experimental $g(E)$, has been adjusted to the low-E_b side of the O $2p$ peak. This procedure is legitimate since the bulk, as well as the surface DOS, abruptly increases at $E_b > 0$ eV. This curve was then subtracted from the experimental spectrum, yielding the contribution of the surface band-gap states. For sputtered surfaces, this peak tails into the band gap, and a low-intensity emission is detectable up to the Fermi level. In this case, the energy difference between VBM and emission at E_F amounts to 3.4 eV. This indicates that the conduction-band minimum (CBM) is close to the Fermi level at the surface. This can be explained by the creation of an accumulation layer at the surface following ion bombardment. The ionized oxygen vacancies created by the bombardment are distributed over a restricted depth of a few ten angstroms, a value much smaller than the Debye length associated with the space-charge layer in tin dioxide.[27] They act as positive charges at the surface and are responsible for the accumulation layer.

An independent confirmation of the existence of an accumulation layer was given by the determination of the work function of our sputtered sample. It could be inferred from the low–kinetic-energy cutoff of the EDC, provided that the vacuum level of our sample lies above that of the spectrometer (4.9 eV). Since the sample work function was usually lower than 4.9 eV, it was necessary to use a fixed negative bias on the sample. The work function determined in this way indicated that the Fermi level was nearly coincident with the low-E_b emission cutoff in the band gap. This implies that a continuous tail of states occurs up to the Fermi level throughout most of the band gap. Since the spectrometer work function is known, the changes in the band bending at the surface could be inferred simply from the kinetic energy at which the VBM appears. The kinetic energy of the emission at VBM for the "perfect" (1×1) surface annealed at 1000 K was taken as a reference, although it may not represent the "flat-band" condition. The inset of Fig. 3 shows that annealing at 800 K slightly increases the band bending which is maximum for the (4×1) surfaces. Further annealing at higher temperatures leads to a decrease in the positive band bending, corresponding to a reduction of the downward curvature of the bands. The variations of the band bending indicate that the surface positive charge, due to ionized oxygen vacancies, is maximum for the (4×1) reconstruction. This can be understood in the following way. For the sputtered surface, the stoichiometry in the perturbed layer created by the bombardment deviates from that of SnO_2. As discussed in Sec. IV B, the oxygen deficiency probably induces a change in the tin oxidation state to Sn^{2+}, as suggested earlier by Cox *et al.*,[12] on the basis of UPS measurements, and by de Frésart,[9(b)] on the basis of surface conductance and contact potential measurements. In this way, an oxygen vacancy adjacent to an Sn^{2+} ion is left neutral. Charged oxygen vacancies will appear upon crystallization of the perturbed layer. This process is complete when the (4×1) reconstruction appears. The oxidation state of the bulk tin ions in this layer is most probably Sn^{4+}, except perhaps at the surface, where half of the tin cations of the compact termination are left in a Sn^{2+} state. It then follows that the remaining oxygen vacancies act as donors. Their ionization at room temperature is responsible for the increased downward band bending. Upon annealing at 900 K, oxygen diffusion from the bulk eliminates the oxygen deficiency near the surface, as reflected by the (1×1) reconstruction. Consequently, the ionized donors related to the oxygen vacancies disappear, and the band bending is decreased. Further annealing at 1000 K is believed to reduce the concentration of charged defects by the progressive filling of oxygen vacancies. The band bending, accordingly, follows the surface charge variations and decreases toward flat-band conditions.

In order to follow in a meaningful way the small changes in the VB shape that occur after each preparation, it was found useful to compute difference curves. The original spectra were aligned with respect to the VBM, normalized before taking their difference. We assumed that we could normalize our spectra to the amplitude of the tin $4d$ signal, which was practically not affected by the surface treatments. Indeed, the tin surface concentration was not crucially affected, even by ion bombardment, contrary to what happens when oxygen suffers preferential sputtering. The amplitude of the Sn $4d$ signal will just reflect the density of cations within a few mean free paths of the photoelectrons. Three difference curves in Fig. 4 have been obtained by subtracting the EDC, taken at $h\nu=40$ eV for the annealed surfaces, from the EDC for the sputtered surface. Two of them show a positive peak corresponding to the reduction of the band-gap states upon annealing. This peak at 1.4 eV above the VBM extends deeper into the band gap after sputtering. All of the curves also indicate two minima in the VB region; the first is located around $E_b=7$ eV, and the other extends from 6 to 0 eV, with a prominent peak value near 0.5 eV. These structures reflect the drop of the DOS resulting, for each main contribution to the VB, from the reduction in the surface oxygen concentration. The shape is similar to that observed by Göpel, Bauer, and Hansson[28] on ZnO surfaces. This is not unexpected since the two compounds have comparable ionicity: Their electronic structures are mainly determined by the coupling between anion-p and metal-s orbitals. Munnix and Schmeits have suggested that UPS difference spectra should yield meaningful informations on the surfaces of different atomic composition or defect structures.[8] By summing the local DOS over the last layers, and by taking the difference between local DOS for defective and perfect surfaces, they were able to simulate theoretical difference curves that can be compared with the experimental ones. This comparison can be made with the assumption that the DOS contribution from deeper layers is the same for both defective and defect-free surfaces. Our results are in good agreement with their simulation[8] regarding the whole valence band, except that the peak above the VBM is in no case predicted by the theory, even if complicated defect geometries on the unrelaxed surface are taken into account. Furthermore, in the case of oxygen-terminated surfaces only, a

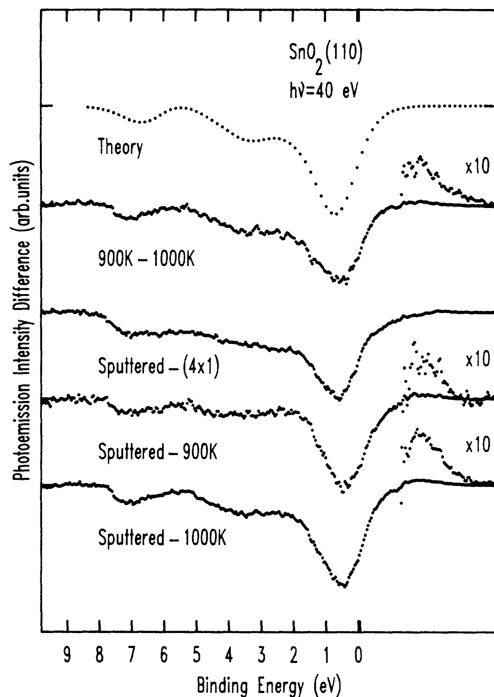

FIG. 4. Difference curves taken from the EDC's of Fig. 3. The intensities of the spectra of Fig. 3 have been calibrated with respect to the same Sn $4d$ intensity. The upper curve represents the calculated difference between the DOS for the compact termination and that for the bridging-oxygen termination (see text for details). The band-gap region is shown on a magnified scale when the difference in the density of band-gap states is significant.

distinct minimum was found in the calculations near $E_b = 3.6$ eV. This structure is precisely found at the same energy only in the difference curve sputtered $(1\times1)-1000$ K of Fig. 4. The other two difference curves show flat or monotonic behavior and no structures at all near 3.6 eV. This favors the hypothesis that, upon annealing at 1000 K, an appreciable fraction of the surface is terminated with a layer of bridging oxygens. That fraction is maximum for the 1000-K annealed surface and much smaller for the 900-K annealed surface, which is best viewed as terminated mostly by a compact plane. In order to check this hypothesis, we show in Fig. 4 the difference curve[17] between the theoretical DOS (Ref. 8) for the compact termination and that for the bridging oxygens termination. Excellent agreement is obtained when these theoretical results are compared with the difference between the EDC for the (1×1) 900-K and that for the (1×1) 1000-K surface. This provides a clear link between the density of bridging oxygen vacancies and of the band-gap states, which are reduced when, after annealing at 1000 K, the DOS at 3.6 eV is well marked.

VI. Sn 4*d* PARTIAL YIELD

The interest in the study of unoccupied electronic states in solids is steadily growing. The validity of one-electron band calculations for describing empty electronic states through absorption thresholds has been questioned, especially in the case of semiconductors or insulators, where the influence of the core-hole potential created during the excitation process and the relaxation of the system can greatly modify the absorption shape through excitonic effects. Nevertheless, other authors have shown that TB (Ref. 24) or spherical-wave calculations[29] can be used to describe x-ray absorption spectra (XANES). For SnO_2, TB calculations predict states of tin $5p$ origin in the conduction band from 7 to 14 eV above the VBM, with a maximum near 12 eV. The optical absorption should thus be observed for $33 < h\nu < 41$ eV, taking into account the E_b of the $4d$ levels and their spin-orbit splitting and gap energy.

The ultraviolet absorption spectrum was measured in the CFS mode of photoemission, also called partial-yield spectroscopy if the kinetic energy is sufficiently low to select slow secondary electrons. This technique is known to provide information on the absorption coefficient $\mu(h\nu)$ closely related to those obtained in a classical optical absorption experiment.[30] Figure 5 shows partial-yield spectra for the sputtered surface at energies E^* of 5, 7, and 9 eV. The spectra have been corrected for the variation in light intensity from the monochromator.

Essentially two types of structures can be distinguished in Fig. 5 according to their behavior with respect to the final (kinetic) energy. The structures of the first type re-

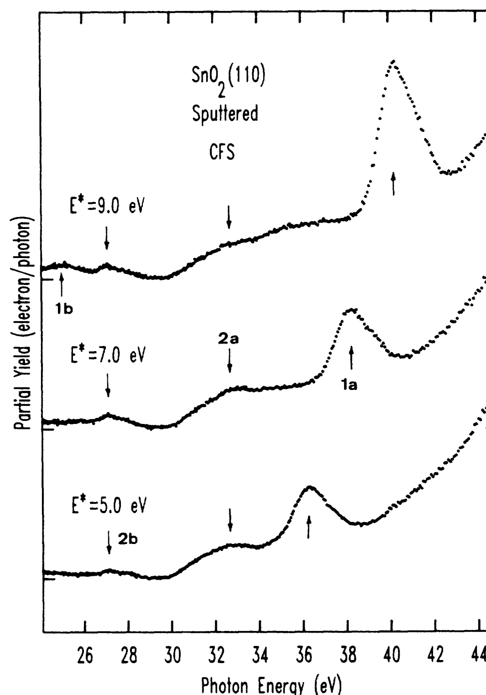

FIG. 5. Partial-yield spectra for final energies of 5.0, 7.0, and 9.0 eV, across the Sn $4d \rightarrow 5p$ transition. The curves have been normalized to their value at $h\nu = 33$ eV. The prominent peak is due to direct photoemission from Sn $4d$ levels. The arrow denotes core excitonic structures associated with the Sn $4d$ core exciton. The signification of the arrows lettering is as follows: (1a) direct photoemission from Sn $4d$ levels; (1b) direct photoemission from Sn $5s$–O $2p$ levels; (2a) maximum of Sn $4d \rightarrow 5p$ absorption; (2b) excitonic features.

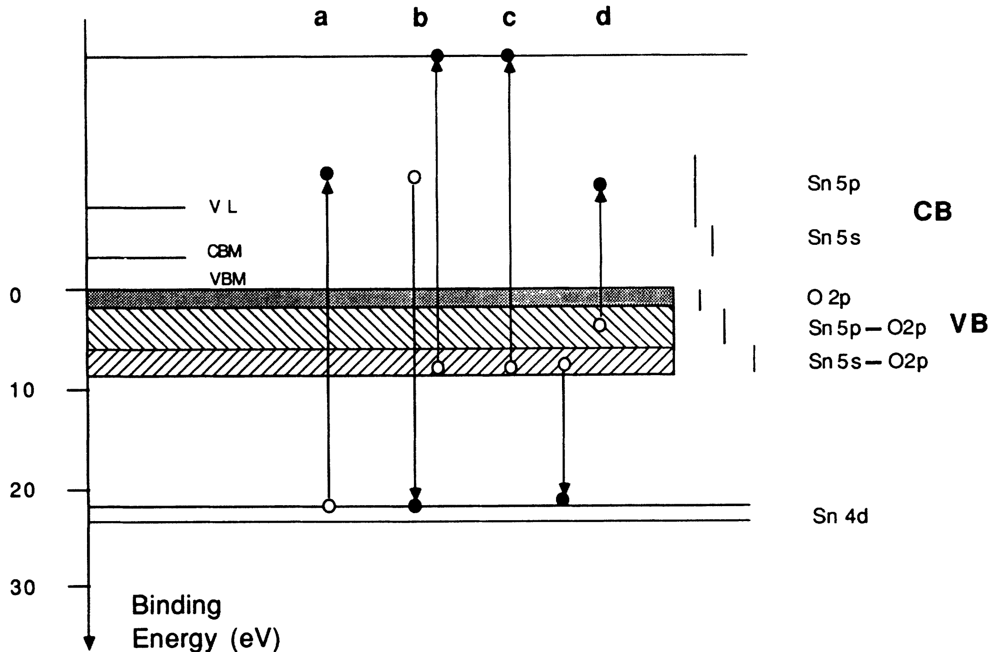

FIG. 6. Schematic energy-level diagram for SnO_2 and illustration of the resonant photoemission processes. (a) Absorption, dipole-allowed transition Sn $4d \rightarrow 5p$. (b) Direct recombination: An electron from tin 5s levels, for example, has been ejected. (c) Direct photoemission from tin 5s levels. Note that the final kinetic energy is the same for the latter two processes. (d) Recombination by Auger decay. VL is the vacuum level.

sult from the usual process of photoemission and shift to higher photon energy when the final energy increases. This is the case for the prominent peak (1a) due to photoemission from Sn 4d levels. Photoemission from the Sn 5s–O 2p states in the VB can be detected as a peak at a photon energy of 25 eV in the 9-eV final energy spectrum (1b). The second type of structure remains fixed when the final energy is changed and consists mainly of a broad peak starting at 30 eV with a clear maximum at 32.5 eV (2a). This enhancement in the partial yield happens when $h\nu$ crosses the $4d \rightarrow 5p$ absorption threshold, a dipole-allowed transition. The empty Sn 5p levels are thus experimentally located starting from 8 eV above VBM, with a maximum near 10 eV. The experimental position of empty Sn 5p states is in qualitative agreement with one-electron calculations. The increase in the partial yield above 36 eV can be ascribed to transitions from Sn 4d to empty Sn 4f levels, which are expected to show up with more intensity than the $4d \rightarrow 5p$ transitions. Above the threshold, optical absorption promotes a 4d electron toward an unoccupied 5p state, which then decays via subsequent Auger or direct recombination processes and their associated secondaries. These mechanisms, to be described in more detail in Sec. VII, are represented in Fig. 6 for the case of tin dioxide in a schematic energy-level diagram. They add supplementary electrons to those produced by the direct photoemission process, leading to an enhancement of the partial yield.

It should be mentioned that some excitonic effects are present for transitions between Sn 4d levels and CBM ($h\nu$=27 eV). The arrow in Fig. 5 denotes a small sharp structure appearing at fixed photon energies which coincide with these transition energies (2b). While the structure at 32.5 eV is essentially the same for every kind of surface preparation, the small excitonic feature only appears on sputtered surfaces. As the states at the CBM are derived from Sn 5s states, the oscillator strength for the transition is weak, and the excitonic peaks may be ascribed to some residual 5p DOS characteristic of the sputtered surface.[31]

VII. RESONANT PHOTOEMISSION

The process of resonant photoemission (RP) has been the subject of numerous investigations devoted mainly to 3p (Ref. 32) and 2p (Ref. 33) thresholds of transition metals and of their compounds. It yields also a method for isolating the d-state contribution to complex hybridized ligand states.[34–36] In the field of metal-semiconductor interfaces, RP has been used to identify the contributions of different chemical elements to the VB.[37] It was recently applied to the high-T_c superconductors, where it helps to study the partial density of filled[38] as well as empty states.[39] In the present work, resonant photoemission from tin states occurs when the photon energy crosses the $4d \rightarrow 5p$ absorption threshold.

The $4d \rightarrow 5p$ transition creates an excited state, consisting of a hole in the 4d shell and an additional electron in the 5p shell of the same atom [(a) in Fig. 6]. The 4d excitation remains localized on the cation site since the 4d orbital does not directly participate in the bonding. There-

fore it is legitimate to describe the following mechanisms as quasiatomic. The optical absorption is thus

$$4d^{10}5p^0(C)+h\nu\rightarrow[4d^95p^1(C)]^* ,$$

where $5p^0(C)$ and $5p^1(C)$ are, respectively, unfilled and filled states in the conduction band,[40] and $h\nu$ is a photon of energy above the threshold. The excited state can relax along two ionization channels that are responsible for the increase in the number of secondaries detected in our partial-yield spectra. The first one is autoionization,[41]

$$[4d^95p^1(C)]^*\rightarrow[4d^95p^0(C)]^*+e^-(E_k') ,$$

followed by an Auger decay [(d) in Fig. 6],

$$[4d^9(V)^n5p^0(C)]^*\rightarrow 4d^{10}(V)^{n-2}5p^0(C)+e^-(E_k'') ,$$

where (V) denotes states in the VB, and E_k'' is the kinetic energy of the electron resulting from the $N_{4,5}VV$ Auger process. The second possible nonradiative mechanism is direct recombination [(b) in Fig. 6], following

$$[4d^9(V)^n5p^1(C)]^*\rightarrow 4d^{10}(V)^{n-1}5p^0(C)+e^-(E_k) .$$

The final state of this process and the kinetic energy of the emitted electron are the same as in the conventional photoemission process [(c) in Fig. 6], namely,

$$4d^{10}(V)^n+h\nu\rightarrow 4d^{10}(V)^{n-1}+e^-(E_k) .$$

In quantum-mechanical terms, the direct recombination interferes with the photoemission process from the VB state, which gives rise to an oscillation in the photoelectron intensity as one sweeps photon energy through the $4d\rightarrow 5p$ threshold. For atomic systems at least, this resonant enhancement is best described by a characteristic Fano line shape.[42] The transitions to empty $4f$ levels detected in the partial-yield spectra do not lead to any resonance. The excited state $[4d^9(V)^n4f^1(C)]^*$ therefore relaxes primarily by Auger decay.

The EDC's of Fig. 7, measured between $24<h\nu<50$ eV, globally show the resonant behavior of photoemission from the various Sn-derived states in the VB of sputtered SnO_2. The sputtered surface was chosen to enhance the contribution from the band-gap states. Each EDC has been normalized to a constant photon flux, and an integral background due to secondary electron has been subtracted from the experimental curves. The spectrum taken at $h\nu=24$ eV contains Sn $4d$ contribution excited with second-order light and gives an unreliable shape for the gap states. Since the Auger electrons referred to above appear at fixed, low kinetic energies, they will not contribute to this series of EDC's.[43] Lad and Henrich[35] have pointed out the problem caused by the resonant behavior of the inelastic electron background, which may be different from the one characterizing the feature of interest. To overcome this problem, we followed their procedure and generated spectra equivalent to the usual CIS (constant initial state) spectra (where the kinetic energy is swept synchronously with photon energy, keeping $h\nu-E_k$ constant) by taking the maximum of the feature of interest at E_b of 6.3 (Sn $5s$), 3.5 (Sn $5p$), and 0.5 (O $2p$) eV directly from our EDC's, where the inelastic background has been subtracted. The contribution from the

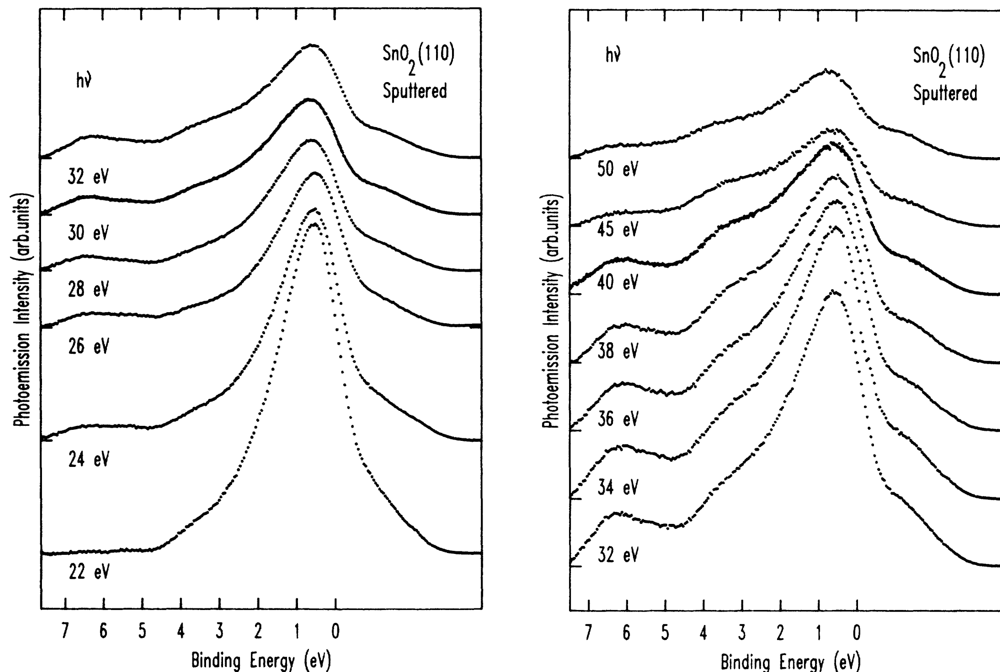

FIG. 7. Valence-band EDC's at various photon energies measured from $SnO_2(110)$ after sputtering, showing the resonant enhancement of the tin-derived states. The inelastic background has been subtracted from the experimental curves. These curves have been normalized to a constant photon flux, which is different for each of the two parts in order to optimize legibility.

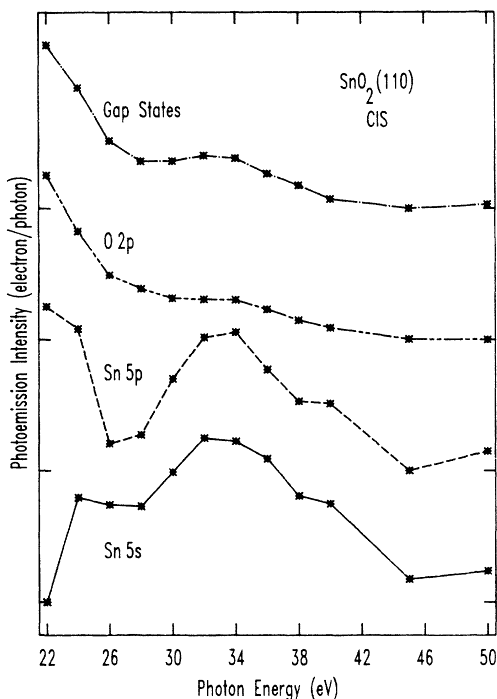

FIG. 8. CIS spectra reconstructed from the EDC's of Fig. 7, corresponding to the three parts of the VB and to the band-gap states (see Sec. VII for details). The photon energy is swept through the Sn $4d \rightarrow 5p$ excitation threshold. Each spectrum has been normalized to its maximum.

surface states which overlap the O $2p$ peak has been extracted using the procedure described in Sec. V, i.e., by subtracting half of a Gaussian adjusted to the leading edge of the O $2p$ peak from the experimental values. The contribution of the band-gap states was then summed to obtain their area. Figure 8 shows these CIS spectra, which originate from the three parts of the VB and from the band-gap states.

In order to use resonant photoemission to identify metal-derived states in oxides and to check the validity of known hybridization scheme for a particular compound, the essential assumption that the direct recombination mechanism is purely intra-atomic has been made[32,36] and appears to be valid. Only in a few cases has an interatomic direct recombination with a resonance of oxygen states been reported, namely, for Ti_2O_3,[34] and (to a smaller extent) V_2O_3, and was observed for the first time in TiO_2,[41] where it has been correlated to photon- and electron-stimulated ion desorption.[44] Furthermore, the observation of excitonic effects is a further argument in favor of a strong localization of the core hole on its tin site and its subsequent intra-atomic recombination. Indeed, it can be seen from Fig. 8 that the O $2p$ levels do not exhibit any resonance at all, which clearly establishes the intra-atomic picture of the direct recombination process. The small bump at $E_b = 34$ eV is most probably due to the resonance of the Sn $5p$ states, which are close to the O $2p$ peak and which still contribute to the O $2p$ maximum. The Sn $5p$ states exhibit a resonance profile closer to a Fano line shape superimposed on a decreasing contribution due to the influence of the O $2p$ levels. The Sn $5p$ states resonant behavior exhibits a minimum near 26 eV and a maximum around 34 eV. The resonant behavior for Sn $5s$ (hybridized with O $2p$ states, $E_b = 7$ eV) cannot be described by a simple Fano line shape. After a sharp increase between 22 and 24 eV, the resonance profile reaches a maximum around 34 eV. The emission from the gap states also exhibits at resonance between 26 and 36 eV, a structure superimposed on a decreasing curve. Since the direct recombination mechanism of the excited state $[4d^9 5p^1(C)]^*$ is purely intra-atomic, any observed resonance must be assigned to Sn-derived states.

This constitutes a clear experimental indication that the band-gap states that appear on defective $SnO_2(110)$ surfaces are Sn derived. In order to explain their origin, we consider again the assumption that the oxygen deficiency in the sputtered layer induces a change of the tin oxidation state from Sn^{4+} to Sn^{2+}. The band structure of this perturbed layer must be nearer to that of SnO. To our knowledge, no band-structure calculation of tin monoxide has ever been published. Nevertheless, on the basis of electron counting only, and starting from the well-known SnO_2 band structure, two additional electrons are able to occupy the next available states at higher energy, which are tin $5s$ states. Electron correlation effects will obviously modify the band structure, but we may reasonably think that the upper states will remain mainly of Sn $5s$ character. We think that this is actually the origin of the tin-derived gap states. It is not essential to invoke any $5s$-$5p$ rehybridization, as suggested earlier,[12] to explain the origin of gap states, although some hybridization with other (oxygen) states is likely to happen. The next unoccupied states in the SnO band structure could be Sn $5p$ states, possibly separated from Sn $5s$ states by a band gap. This could explain why excitonic features are seen in our partial-yield spectra for sputtered surfaces. In this case, the Sn $5p$ states near the conduction-band minimum are responsible for the enhanced oscillator strength of the dipole-allowed Sn $4d \rightarrow 5p$ transition. Further experimental work is currently in hand to test this hypothesis.[31] Modifications of electron correlation effects, resulting from the change of the tin oxidation state, could also explain the failure of TB-based methods to predict the occurrence of the band-gap states. These methods are dealing with a DOS which is actually frozen and does not change upon electron occupancy. In the case of SnO_2, more elaborate methods, which take into account the electron occupancy in a self-consistent way, should be used to reconcile theory with experiment.

VIII. SUMMARY AND CONCLUSIONS

The electronic properties of $SnO_2(110)$ surfaces have been studied. The major conclusions of this work are the following:

There is a good agreement between our EDC's and the calculated local-DOS on (1×1) (110) surfaces. The VB width is of 7.5 eV. The comparison of DOS calculations for defective surfaces, with the difference curves between EDC's for different surface treatments, shows up the

differences between the compact plane or bridging-oxygen-terminated surfaces. The key aspect is that a part of the tin cations near the surface change their oxidation state from Sn^{4+} to Sn^{2+}. These Sn^{2+} ions are present in the depth of the layer perturbed by the ion bombardment following oxygen preferential sputtering and the loss of stoichiometry. Sn^{2+} ions are also present at half of the tin sites at the surface, following recrystallization and annealing up to more than 900 K (compact termination). Further annealing at higher temperatures (1000 K) reduces the concentration of Sn^{2+} ions, and oxygen diffusion from the bulk gradually induces a bridging-oxygen termination. The shape of the EDC's involving emission from the Sn 4*d* core level also supports our interpretation.

The band-gap surface states, which were not predicted by TB calculations, have been precisely localized at 1.4 eV above the VBM. Resonant photoemission from cation states (including band-gap states) has been observed as the photon energy is swept through the $4d \rightarrow 5p$ transition. This demonstrates the tin-derived character of the band-gap states, which are also tentatively assigned to Sn 5*s* states from Sn^{2+} ions, in the surface region. Unoccupied Sn 5*p* states in the conduction band with a maximum at 10 eV above VBM were also localized using partial-yield spectra. Residual Sn 5*p* states near the CBM were found for sputtered surfaces through core excitonic effects.

ACKNOWLEDGMENTS

This research was initiated with the support of Professor M. Cardona. We are grateful to Dr. M. Schmeits for comments and discussion and for communicating unpublished results. This work was supported by the Belgian Fund for Scientific Research (FNRS), the Belgian Ministry for Science Policy (SPPS) through IRIS concerted actions, the Interuniversity Research Project in Interface Sciences (PAIT-ISIS), and the Bundesministerium für Forschung und Technologie (BMFT, Project No. 05 490 CAB). R.S. acknowledges financial support from the Belgian National Fund for Scientific Research.

---

*Also at Laboratoire Interdépartemental de Spectroscopie Electronique (LISE), Institute for Studies in Interface Sciences (ISIS), Facultés Universitaires Notre Dame de la Paix, 61 rue de Bruxelles, B-5000 Namur, Belgium.

[1]V. E. Henrich, Rep. Prog. Phys. **48**, 1481 (1985).
[2]G. Heiland and H. Lüth, in *The Chemical Physics of Solid Surfaces and Heterogeneous Catalysis,* edited by D. A. King and D. P. Woodruff (Elsevier, Amsterdam, 1984), Vol. III, Chap. 4.
[3]J. Watson, Sensors and Actuators **5**, 29 (1984).
[4]Ch. Tatsuyama, Sh. Ichimura, and H. Iwakuro, Jpn. J. Appl. Phys. **21**, L25 (1973).
[5]M. J. Fuller and M. E. Warwick, J. Catal. **29**, 441 (1973).
[6]Z. M. Jarzebski and J. P. Marton, J. Electrochem. Soc. **123**, 199 (1976); **123**, 299 (1976); **123**, 333 (1976).
[7]J. Robertson, J. Phys. C **12**, 4767 (1979).
[8](a) S. Munnix and M. Schmeits, Phys. Rev. B **27**, 7624 (1983); (b) **33**, 4136 (1986).
[9](a) E. de Frésart, J. Darville, and J. M. Gilles, Solid State Commun. **37**, 13 (1980); Appl. Surf. Sci. **11/12**, 637 (1982); Surf. Sci. **126**, 518 (1983); (b) E. de Frésart, Ph.D. thesis, University of Namur, 1983 (unpublished).
[10]D. F. Cox, T. B. Fryberger, and S. Semancik, Phys. Rev. B **38**, 2072 (1988).
[11]R. G. Egdell, S. Eriksen, and W. R. Flavell, Solid State Commun. **60**, 835 (1986).
[12]P. A. Cox, R. G. Egdell, C. Harding, W. R. Patterson, and P. J. Tavener, Surf. Sci. **123**, 179 (1982).
[13](a) P. L. Gobby and G. J. Lapeyre, in *Proceedings of the Thirteenth International Conference on Physics of Semiconductors, Rome, 1976,* edited by F. G. Fumi (North-Holland, Amsterdam, 1976), p. 150; (b) P. L. Gobby, Ph.D. dissertation, Montana State University, 1977 (unpublished), available from University Microfilms International, Ann Arbor, MI.
[14]B. Feuerbacher, B. Fitton, and R. F. Willis, in *Photoemission and the Electronic Properties of Surfaces,* edited by B. Feuerbacher, B. Fitton, and R. F. Willis (Wiley, New York, 1978), p. 12.
[15]R. L. Johnson and J. Reichardt, Nucl. Instrum. Methods **208**, 791 (1983).
[16]B. Thiel and R. Helbig, J. Crystal Growth **32**, 259 (1976).
[17]M. Schmeits (private communications).
[18]J. C. Fuggle and M. Martensson, J. Electron. Spectrosc. Relat. Phenom. **21**, 275 (1980).
[19]See E. A. Kraut, R. W. Grant, J. R. Waldrop, and S. P. Kowalczyk, Phys. Rev. B **28**, 1965 (1983), and references therein.
[20]M. L. Cohen and J. R. Chelikowsky, in *Electronic Structure and Optical Properties of Semiconductors,* Vol. 75 of *Springer Series in Solid-State Sciences,* edited by M. Cardona (Springer-Verlag, Berlin, 1988).
[21]J. Arlinghaus, J. Phys. Chem. Solids **35**, 931 (1974).
[22]J. L. Jacquemin and G. Bordure, J. Phys. Chem. Solids **36**, 1081 (1974).
[23]A. Svane and E. Antoncik, J. Phys. Chem. Solids **48**, 171 (1987).
[24]J. Robertson, Phys. Rev. B **28**, 3378 (1983).
[25]G. Rocker and W. Göpel, Surf. Sci. **181**, 530 (1987).
[26]J. M. McKay and V. E. Henrich, Phys. Rev. B **39**, 6156 (1989).
[27]The equation $L_d = (\epsilon_r \epsilon_0 kT / e^2 n_b)^{1/2}$ has been applied with $\epsilon_r = 9.3$, and $n_b = 10^{16}$ m^{-3}, from bulk conductivity measurements and yields $L_d = 36$ μm.
[28]W. Göpel, R. S. Bauer, and G. Hansson, Surf. Sci. **99**, 138 (1980).
[29]M. T. Czyzyk *et al.*, Phys. Rev. B **39**, 9831 (1989).
[30]See, e.g., C. Kunz, in *Photoemission in Solids II,* Vol. 27 of *Topics in Applied Physics,* edited by L. Ley and M. Cardona (Springer-Verlag, Berlin, 1979), p. 322, and references therein.
[31]J. M. Themlin (unpublished).
[32]For an excellent review, see L. C. Davis, J. Appl. Phys. **59**, R25 (1986).
[33]S. C. Wu, C. K. C. Lok, J. Sokolov, F. Jona, and A. Taleb-Ibrahimi, Phys. Rev. B **39**, 1058 (1989).
[34]K. E. Smith and V. E. Henrich, Phys. Rev. B **38**, 9571 (1988).
[35]R. J. Lad and V. E. Henrich, Phys. Rev. B **38**, 10 860 (1988).
[36]R. J. Lad and V. E. Henrich, J. Vac. Sci. Technol. **A7**, 1893 (1989).
[37]G. Margaritondo and A. Franciosi, Ann. Rev. Mater. Sci. **14**,

67 (1984).
[38]M. W. Ruckman *et al.*, Phys. Rev. B **39**, 7359 (1989).
[39]R. Manzke, T. Buslaps, R. Claessen, G. Mante, and Z. X. Zhao, Solid State Commun. **70**, 67 (1989).
[40]We follow the notations of M. R. Thuler, R. L. Benbow, and Z. Hurych, Phys. Rev. B **26**, 669 (1982).
[41]E. Bertel, R. Stockbauer, and T. E. Madey, Phys. Rev. B **27**, 1939 (1983).
[42]U. Fano, Phys. Rev. **124**, 1866 (1961); U. Fano and J. W. Cooper, Rev. Mod. Phys. **40**, 441 (1968).
[43]The maximum kinetic energy for $N_{4,5}VV$ Auger electrons is 15 eV, assuming that the emitted electron and the one filling the core hole are both coming from the band-gap states. The third part of the VB (Sn $5s$–O $2p$ states) could be affected by the process up to $h\nu=32$ eV, since they are detected at a kinetic energy of 15 eV for a photon energy of 32 eV. The Sn $5p$–O $2p$ states could be affected up to $h\nu=28$ eV, and the O $2p$ states up to $h\nu=25$ eV. However, an Auger structure would be seen at increasing photon energies in our CIS spectra as the initial energy is increased. No structures with a similar behavior can be distinguished in Fig. 8.
[44]T. E. Madey, D. E. Ramaker, and R. Stockbauer, Ann. Rev. Phys. Chem. **35**, 215 (1984).

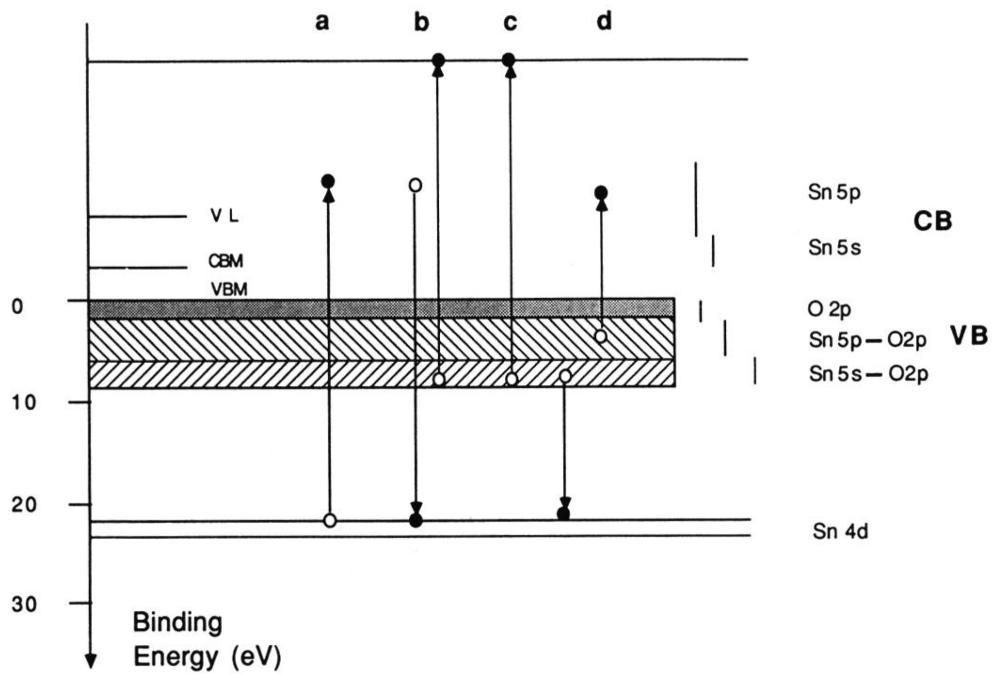

FIG. 6. Schematic energy-level diagram for SnO_2 and illustration of the resonant photoemission processes. (a) Absorption, dipole-allowed transition Sn $4d \rightarrow 5p$. (b) Direct recombination: An electron from tin $5s$ levels, for example, has been ejected. (c) Direct photoemission from tin $5s$ levels. Note that the final kinetic energy is the same for the latter two processes. (d) Recombination by Auger decay. VL is the vacuum level.